Nonequilibrium behavior of the kinetic metamagnetic spin-5/2 Blume–Capel model

Ümüt Temizer†

Department of Physics, Bozok University, Yozgat 66200, *Turkey*

(Received 19 July 2013; revised manuscript received 29 November 2013; published online 28 May 2014)

The dynamic magnetic behavior of the kinetic metamagnetic spin-5/2 Blume–Capel model is examined, within a mean-field approach, under a time-dependent oscillating magnetic field. To describe the kinetics of the system, Glauber-type stochastic dynamics has been utilized. The mean-field dynamic equations of the model are obtained from the Master equation. Firstly, these dynamic equations are solved to find the phases in the system. Then, the dynamic phase transition temperatures are obtained by investigating the thermal behavior of dynamic sublattice magnetizations. Moreover, from this investigation, the nature of the phase transitions (first- or second-order) is characterized. Finally, the dynamic phase diagrams are plotted in five different planes. It is found that the dynamic phase diagrams contain the paramagnetic (P), antiferromagnetic ($AF_{5/2}$, $AF_{3/2}$, $AF_{1/2}$) phases and five different mixed phases. The phase diagrams also display many dynamic critical points, such as tricritical point, triple point, quadruple point, double critical end point and separating point.

Keywords: metamagnetism, spin-5/2 Blume–Capel model, dynamic phase transitions, dynamic phase diagrams, Glauber-type stochastic dynamics

PACS: 05.70.Fh, 75.10.Hk, 74.40.Gh, 75.30.Kz **DOI:** 10.1088/1674-1056/23/7/070511

1. Introduction

The metamagnetic systems are systems in which antiferromagnetic and ferromagnetic interactions exist simultaneously. $FeCI_2$ and $FeBr_2$ are well-known metamagnets of the Ising type.[1–4] The equilibrium properties of Ising metamagnets have been investigated in detail.[5–17] On the other hand, the dynamic magnetic behavior of the metamagnetic systems has been a subject of interest for a long time. Yang[18] studied the kinetic spin-1/2 metamagnetic Ising system by using Glauber dynamics.[19] Zukovic and Idogaki[20] have investigated the magnetic properties of a diluted spin-1/2 Ising metamagnet by using Monte Carlo (MC) simulations. Sahni *et al.*[21] employed MC simulations with Kawasaki dynamics to investigate the dynamic behavior of the Ising metamagnet. Oğuz[22] investigated the spin-1/2 Ising metamagnetic system by using the dynamic MC renormalization group (RG) method. From this investigation, the exactly tricritical point value was obtained. Santos and Figueiredo[23] studied the spin-1/2 metamagnetic Ising system on a square lattice through the master-equation formalism and considered the stochastic Glauber process within the dynamical pair approximation. Das and Barma[24] investigated the dynamic magnetic properties of the system in the absence of the external magnetic field by using three-spin flip dynamics. Gülpınar *et al.*[25,26] studied the dynamics of the Ising metamagnet under a time-dependent oscillating magnetic field by Glauber dynamics. Keskin *et al.*[27–29] have investigated the nonequilibrium aspects of spin-1,[27] spin-3/2 Blume–Capel (BC)[28] and spin-3/2 Blume–Emery–Griffiths (BEG)[29] metamagnetic Ising systems by using the dynamic mean-field approximation (MFA) based on Glauber dynamics. Gülpınar[30] calculated the sound attenuation coefficient of a spin-1/2 metamagnetic Ising system by the thermodynamics of irreversible processes. Deviren and Keskin[31] examined the dynamic aspects of a two-sublattice Ising metamagnet on honeycomb, square and hexagonal lattices under the oscillating magnetic field by using the effective field theory (EFT) with correlations. Acharyya[32] studied the dynamic responses of an Ising metamagnet in the presence of the sinusoidal magnetic field by the MC simulations. Finally, Gülpınar and Vatansever[33] have studied the steady state solutions of the spin-1/2 metamagnetic Ising model under a time-dependent oscillating external physical and staggered magnetic fields.

Although the majority of the studies mentioned above have focused on spin-1/2, spin-1 and spin-3/2 Ising systems, higher spin systems are not without interest. One of the important higher spin systems is a spin-5/2 Ising model. A spin-5/2 Ising model is a six-state spin model, namely, $S = \pm 5/2, \pm 3/2, \pm 1/2$. The equilibrium properties of the spin-5/2 Ising model have been investigated by using the MFA, EFT, mean-field renormalization group theory (MFRG) and MC simulations (see Refs. [34]–[43] and references therein). While considerable progress has been made in understanding the equilibrium properties of the spin-5/2 Ising model, the nonequlibrium properties of the model have not been explored thoroughly. There have been only few studies on the dynamical aspects of the model.[44–49]

To the best of the author's knowledge, the dynamic mag-

†Corresponding author. E-mail: umut.temizer@bozok.edu.tr

© 2014 Chinese Physical Society and IOP Publishing Ltd

netic behavior of the metamagnetic spin-5/2 Ising model has not been studied so far. The purpose of this work is to study the nonequilibrium behavior of the kinetic metamagnetic spin-5/2 Ising model with bilinear (J) and crystal-field interactions (D) under the time-dependent oscillating external magnetic field. For this purpose, firstly, the mean-field dynamic equations are constructed by using the Glauber transition rates. These equations are solved to find the phases in the system. Then, the dynamic phase transition (DPT) temperatures are obtained by investigating the thermal behavior of the dynamic sublattice magnetizations. As a result of these investigations, dynamic phase diagrams are presented in five different planes. It is worthwhile mentioning that the dynamic phase diagrams in the $(-\alpha,T)$, (d,h), and $(-\alpha,h)$ planes for the metamagnetic Ising systems will be given in this study, firstly.

The paper is organized in the following manner. In Section 2, the metamagnetic spin-5/2 BC model is briefly described and the derivation of the mean-field dynamic equations is given by using the Glauber-type stochastic dynamics in an oscillating magnetic field. Numerical results and discussion are presented in Section 3. The paper ends with a summary and conclusion in Section 4.

2. Model and formulations

The Hamiltonian of the metamagnetic spin-5/2 Ising model that contains a single-ion potential or crystal-field interaction in addition to the bilinear exchange interaction, also called the Blume–Capel (BC) model, is given by

$$\begin{aligned}\mathcal{H} = & -J\sum_{\mathrm{nn}} S_iS_j - J'\sum_{\mathrm{nnn}} S_iS_k \\ & -D\left(\sum_{i=1}^{N} S_i^2+\sum_{j=1}^{N} S_j^2\right) - H\left(\sum_{i=1}^{N} S_i+\sum_{j=1}^{N} S_j\right). \quad (1)\end{aligned}$$

In this Hamiltonian, the first term describes the antiferromagnetic exchange constant ($J<0$) with the nearest neighbor spin (nn) in the neighboring layers. The second term denotes the ferromagnetic exchange interaction ($J'>0$) of some considered spin with the next-nearest neighbors spins (nnn) in its layer. The D is the crystal-field interaction or a single-ion anisotropy constant and H is a time-dependent oscillating external magnetic field. The H is given by

$$H(t) = H_0\cos(wt), \quad (2)$$

where H_0 and $w=2\pi\upsilon$ are the amplitude and the angular frequency of the oscillating field, respectively. The system is in contact with an isothermal heat bath at absolute temperature T.

The Glauber transition rates are employed to construct the set of mean-field dynamic equations. The system evolves according to a Glauber-type stochastic process at a rate of $1/\tau$ transitions per unit time; hence the frequency of spin flipping, f, is $1/\tau$. $P(S_1,S_2,\ldots,S_N;t)$ is defined as the probability function such that the system has the S-spin configuration $S_1,S_2,\ldots,S_N$ at time t. The time dependence of this probability function is assumed to be governed by the master equation which describes the interaction between spins and the heat bath. In Glauber dynamics, the transition probabilities of the individual spins are assumed to depend on the momentary values of the neighboring spins as well as on the influence of the heat bath. $W_i(S_i\to S_i')$ is the transition probability per unit time that the i-th spin changes from the value S_i to S_i' while the others remain momentarily fixed. Therefore, if the spins on sublattice B remain momentarily fixed, the master equation for sublattice A can be written as

$$\begin{aligned}&\frac{\mathrm{d}}{\mathrm{d}t}P^{\mathrm{A}}(S_1,S_2,\ldots,S_N;t) \\ &= -\sum_i\left(\sum_{S_i\neq S_i'} W_i^{\mathrm{A}}(S_i\to S_i')\right) \\ &\quad\times P^{\mathrm{A}}(S_1,S_2,\ldots,S_i,\ldots,S_N;t) \\ &\quad+\sum_i\left(\sum_{S_i\neq S_i'} W_i^{\mathrm{A}}(S_i'\to S_i)\right) \\ &\quad\times P^{\mathrm{A}}(S_1,S_2,\ldots,S_i',\ldots,S_N;t). \quad (3)\end{aligned}$$

Since the system is in contact with a heat bath at absolute temperature T, each spin can change from the value S_i to S_i' with the probability per unit time

$$W_i^{\mathrm{A}}(S_i\to S_i') = \frac{1}{\tau}\frac{\exp\left(-\beta\Delta E^{\mathrm{A}}(S_i\to S_i')\right)}{\sum_{S_i'}\exp\left(-\beta\Delta E^{\mathrm{A}}(S_i\to S_i')\right)}, \quad (4)$$

where $\beta=1/k_{\mathrm{B}}T$, k_{B} is the Boltzmann factor, $\sum_{S_i'}$ is the sum over the six possible values of $S_i'=\pm5/2,\pm3/2,\pm1/2$, and

$$\begin{aligned}\Delta E^{\mathrm{A}}(S_i\to S_i') = & -(S_i'-S_i)\left(J\sum_{\mathrm{nn}} S_j + J'\sum_{\mathrm{nnn}} S_k + H\right) \\ & -\left[(S_i')^2-(S_i)^2\right]D \quad (5)\end{aligned}$$

is the change in the energy of the system when the S_i spin changes, which can be found by using Eq. (1). Using the detailed balance condition,[28,29] we obtain

$$W_i^{\mathrm{A}}\left(\frac{3}{2}\to\frac{5}{2}\right) = W_i^{\mathrm{A}}\left(\frac{1}{2}\to\frac{5}{2}\right) = W_i^{\mathrm{A}}\left(-\frac{1}{2}\to\frac{5}{2}\right) = W_i^{\mathrm{A}}\left(-\frac{3}{2}\to\frac{5}{2}\right) = W_i^{\mathrm{A}}\left(-\frac{5}{2}\to\frac{5}{2}\right)$$

$$= \frac{1}{\tau}\frac{\mathrm{e}^{(2\beta D)}\,\mathrm{e}^{(5\beta x/2)}}{2\mathrm{e}^{(2\beta D)}\cosh(5\beta x/2)+2\mathrm{e}^{(-2\beta D)}\cosh(3\beta x/2)+2\mathrm{e}^{(-4\beta D)}\cosh(\beta x/2)}, \tag{6a}$$

$$W_i^{\mathrm{A}}\left(\frac{5}{2}\to\frac{3}{2}\right) = W_i^{\mathrm{A}}\left(\frac{1}{2}\to\frac{3}{2}\right) = W_i^{\mathrm{A}}\left(-\frac{1}{2}\to\frac{3}{2}\right) = W_i^{\mathrm{A}}\left(-\frac{3}{2}\to\frac{3}{2}\right) = W_i^{\mathrm{A}}\left(-\frac{5}{2}\to\frac{3}{2}\right)$$
$$= \frac{1}{\tau}\frac{\mathrm{e}^{(-2\beta D)}\,\mathrm{e}^{(3\beta x/2)}}{2\mathrm{e}^{(2\beta D)}\cosh(5\beta x/2)+2\mathrm{e}^{(-2\beta D)}\cosh(3\beta x/2)+2\mathrm{e}^{(-4\beta D)}\cosh(\beta x/2)}, \tag{6b}$$

$$W_i^{\mathrm{A}}\left(\frac{5}{2}\to\frac{1}{2}\right) = W_i^{\mathrm{A}}\left(\frac{3}{2}\to\frac{1}{2}\right) = W_i^{\mathrm{A}}\left(-\frac{1}{2}\to\frac{1}{2}\right) = W_i^{\mathrm{A}}\left(-\frac{3}{2}\to\frac{1}{2}\right) = W_i^{\mathrm{A}}\left(-\frac{5}{2}\to\frac{1}{2}\right)$$
$$= \frac{1}{\tau}\frac{\mathrm{e}^{(-4\beta D)}\,\mathrm{e}^{(\beta x/2)}}{2\mathrm{e}^{(2\beta D)}\cosh(5\beta x/2)+2\mathrm{e}^{(-2\beta D)}\cosh(3\beta x/2)+2\mathrm{e}^{(-4\beta D)}\cosh(\beta x/2)}, \tag{6c}$$

$$W_i^{\mathrm{A}}\left(\frac{5}{2}\to-\frac{1}{2}\right) = W_i^{\mathrm{A}}\left(\frac{3}{2}\to-\frac{1}{2}\right) = W_i^{\mathrm{A}}\left(\frac{1}{2}\to-\frac{1}{2}\right) = W_i^{\mathrm{A}}\left(-\frac{3}{2}\to-\frac{1}{2}\right) = W_i^{\mathrm{A}}\left(-\frac{5}{2}\to-\frac{1}{2}\right)$$
$$= \frac{1}{\tau}\frac{\mathrm{e}^{(-4\beta D)}\,\mathrm{e}^{(-\beta x/2)}}{2\mathrm{e}^{(2\beta D)}\cosh(5\beta x/2)+2\mathrm{e}^{(-2\beta D)}\cosh(3\beta x/2)+2\mathrm{e}^{(-4\beta D)}\cosh(\beta x/2)}, \tag{6d}$$

$$W_i^{\mathrm{A}}\left(\frac{5}{2}\to-\frac{3}{2}\right) = W_i^{\mathrm{A}}\left(\frac{3}{2}\to-\frac{3}{2}\right) = W_i^{\mathrm{A}}\left(\frac{1}{2}\to-\frac{3}{2}\right) = W_i^{\mathrm{A}}\left(-\frac{1}{2}\to-\frac{3}{2}\right) = W_i^{\mathrm{A}}\left(-\frac{5}{2}\to-\frac{3}{2}\right)$$
$$= \frac{1}{\tau}\frac{\mathrm{e}^{(-2\beta D)}\,\mathrm{e}^{(-3\beta x/2)}}{2\mathrm{e}^{(2\beta D)}\cosh(5\beta x/2)+2\mathrm{e}^{(-2\beta D)}\cosh(3\beta x/2)+2\mathrm{e}^{(-4\beta D)}\cosh(\beta x/2)}, \tag{6e}$$

$$W_i^{\mathrm{A}}\left(\frac{5}{2}\to-\frac{5}{2}\right) = W_i^{\mathrm{A}}\left(\frac{3}{2}\to-\frac{5}{2}\right) = W_i^{\mathrm{A}}\left(\frac{1}{2}\to-\frac{5}{2}\right) = W_i^{\mathrm{A}}\left(-\frac{1}{2}\to-\frac{5}{2}\right) = W_i^{\mathrm{A}}\left(-\frac{3}{2}\to-\frac{5}{2}\right)$$
$$= \frac{1}{\tau}\frac{\mathrm{e}^{(2\beta D)}\,\mathrm{e}^{(-5\beta x/2)}}{2\mathrm{e}^{(2\beta D)}\cosh(5\beta x/2)+2\mathrm{e}^{(-2\beta D)}\cosh(3\beta x/2)+2\mathrm{e}^{(-4\beta D)}\cosh(\beta x/2)}, \tag{6f}$$

where $x = J\sum_{\mathrm{nn}} S_j + J'\sum_{\mathrm{nnn}} S_k + H$. Notice that, since $W_i^{\mathrm{A}}(S_i \to S_i')$ does not depend on the value S_i, we can therefore write $W_i^{\mathrm{A}}(S_i \to S_i') = W_i^{\mathrm{A}}(S_i')$. Hence, the master equation becomes

$$\frac{\mathrm{d}}{\mathrm{d}t}P^{\mathrm{A}}(S_1,S_2,\ldots,S_N;t) = -\sum_i\left(\sum_{S_i\neq S_i'} W_i^{\mathrm{A}}(S_i')\right)P^{\mathrm{A}}\left(S_1,S_2,\ldots,S_i,\ldots,S_N;t\right)$$
$$+\sum_i W_i^{\mathrm{A}}(S_i)\left(\sum_{S_i\neq S_i'} P^{\mathrm{A}}(S_1,S_2,\ldots,S_i',\ldots,S_N;t)\right). \tag{7}$$

Multiplying both sides of Eq. (7) by S_k for m_{A} and then taking the average, we obtain

$$\tau\frac{\mathrm{d}}{\mathrm{d}t}\langle S\rangle_{\mathrm{A}} = -\langle S\rangle_{\mathrm{A}} + \frac{5\mathrm{e}^{(2\beta D)}\sinh(5\beta y/2)+3\mathrm{e}^{(-2\beta D)}\sinh(3\beta y/2)+\mathrm{e}^{-4\beta D}\sinh(\beta y/2)}{2\mathrm{e}^{(2\beta D)}\cosh(5\beta y/2)+2\mathrm{e}^{(-2\beta D)}\cosh(3\beta y/2)+2\mathrm{e}^{(-4\beta D)}\cosh(\beta y/2)}, \tag{8}$$

where $y = \jmath\langle S\rangle_{\mathrm{B}} + \jmath'\langle S\rangle_{\mathrm{A}} + H_0\cos(\omega t)$, $\jmath = Jz$, and $\jmath' = J'z'$, z and z' are the coordination numbers for this model. The system evolves according to the differential equation given by Eq. (8) that can be written in the following form in terms of a mean-field approach:

$$\Omega\frac{\mathrm{d}}{\mathrm{d}\xi}m_{\mathrm{A}} = -m_{\mathrm{A}} + \frac{5\mathrm{e}^{2d/T}\sinh(5a/2\alpha T)+3\mathrm{e}^{-2d/T}\sinh(3a/2\alpha T)+\mathrm{e}^{-4d/T}\sinh(a/2\alpha T)}{2\mathrm{e}^{2d/T}\cosh(5a/2\alpha T)+2\mathrm{e}^{-2d/T}\cosh(3a/2\alpha T)+2\mathrm{e}^{-4d/T}\cosh(a/2\alpha T)}, \tag{9}$$

where $a = (m_{\mathrm{B}} + \alpha m_{\mathrm{A}} + \alpha h\cos(\xi))$, $m_{\mathrm{A}} \equiv \langle S\rangle_{\mathrm{A}}$, $m_{\mathrm{B}} \equiv \langle S\rangle_{\mathrm{B}}$, $\alpha = J'/J$, $\xi = \omega t$, $T = (\beta J')^{-1}$, $h = H_0/J'$, $d = D/J'$, and $\Omega = \tau\omega$.

Now, assuming that the spins on sublattice A remain momentarily fixed and the spins on the sublattice B change, we obtain mean-field dynamic equation for the sublattice magnetization m_{B} with the similar calculation as

$$\Omega\frac{\mathrm{d}}{\mathrm{d}\xi}m_{\mathrm{B}} = -m_{\mathrm{B}} + \frac{5\mathrm{e}^{2d/T}\sinh(5b/2\alpha T)+3\mathrm{e}^{-2d/T}\sinh(3b/2\alpha T)+\mathrm{e}^{-4d/T}\sinh(b/2\alpha T)}{2\mathrm{e}^{2d/T}\cosh(5b/2\alpha T)+2\mathrm{e}^{-2d/T}\cosh(3b/2\alpha T)+2\mathrm{e}^{-4d/T}\cosh(b/2\alpha T)}, \tag{10}$$

where $b = (m_{\mathrm{A}} + \alpha m_{\mathrm{B}} + \alpha h\cos(\xi))$. Hence, the set of the mean-field dynamic equations for the sublattice magnetizations is obtained. $J = -1.0$, $\Omega/2\pi = 1.0$, and $z = z' = 4$ are taken in all calculations.

3. Numerical results and discussion

3.1. Time variations of the average sublattice magnetizations

In this section, firstly, the phases in the system will be found by investigating the time variations of the average sublattice magnetizations ($m_{\rm A}(\xi)$ and $m_{\rm B}(\xi)$). For this purpose, the stationary solutions of the dynamic equations, given by Eqs. (9) and (10), should be studied for the different values of T, α, d, and h. The stationary solutions of Eqs. (9) and (10) will be a periodic function of ξ with period 2π, that is,

$$m_{\rm A}(\xi+2\pi)=m_{\rm A}(\xi), \tag{11a}$$

and

$$m_{\rm B}(\xi+2\pi)=m_{\rm B}(\xi). \tag{11b}$$

Moreover, they can be one of two types according to whether they have or do not have the property

$$m_{\rm A}(\xi+\pi)=-m_{\rm A}(\xi), \tag{12a}$$

and

$$m_{\rm B}(\xi+\pi)=-m_{\rm B}(\xi). \tag{12b}$$

Type 1 The first type of solution satisfies Eq. (12) and is called a symmetric solution. This solution corresponds to paramagnetic (P) phase. It occurs at high temperature or at high values of external magnetic field. In this solution, $m_{\rm A}(\xi)$ and $m_{\rm B}(\xi)$ are equal to each other. They oscillate around the zero value and are delayed with respect to the external magnetic field. An example of such a case is shown in Fig. 1(a).

Type 2 The second type of solution which does not satisfy Eq. (12) and is called a nonsymmetric solution. This solution corresponds to an antiferromagnetic (AF) phase. In this case, $m_{\rm A}(\xi)$ and $m_{\rm B}(\xi)$ do not follow the external field and oscillate around the nonzero value. If $m_{\rm A}(\xi)$ and $m_{\rm B}(\xi)$ oscillate around $\pm1/2$ and $\mp1/2$ respectively, this solution is called the antiferromagnetic-1/2 ($\rm AF_{1/2}$) phase; if $m_{\rm A}(\xi)$ and $m_{\rm B}(\xi)$ oscillate around $\pm3/2$ and $\mp3/2$ respectively, this solution is called the antiferromagnetic-3/2 ($\rm AF_{3/2}$) phase; if $m_{\rm A}(\xi)$ and $m_{\rm B}(\xi)$ oscillate around $\pm5/2$ and $\mp5/2$ respectively, this solution is called the antiferromagnetic-5/2 ($\rm AF_{5/2}$) phase. The example for $\rm AF_{5/2}$ phase is given in Fig. 1(b).

On the other hand, there are mixed phase regions in which both phases coexist depending on the interaction parameters and initial values. These regions occur in the system at low values of the temperature. The examples for $\rm AF_{1/2}$+P and $\rm AF_{1/2}+AF_{3/2}+AF_{5/2}$ mixed phase regions are shown in Figs. 1(c) and 1(d), respectively. Moreover, $\rm AF_{5/2}$+P, $\rm AF_{1/2}+AF_{3/2}$, and $\rm AF_{1/2}+AF_{5/2}$ mixed phase regions also exist in this system.

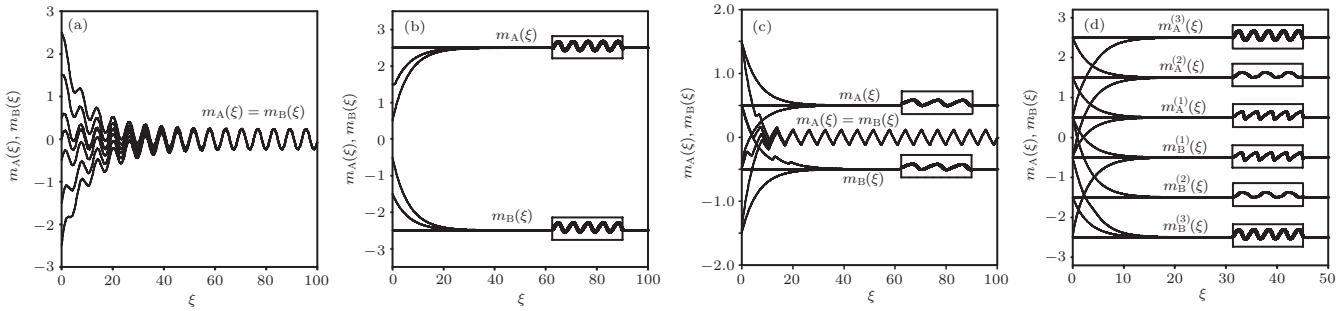


Fig. 1. Time variations of the average sublattice magnetizations ($m_{\rm A}(\xi)$ and $m_{\rm B}(\xi)$): (a) A paramagnetic phase (P) for $\alpha=-0.1$, $d=-2.5$, $h=2.2$, and $T=1.4$. (b) An antiferromagnetic-5/2 phase ($\rm AF_{5/2}$) for $\alpha=-0.5$, $d=5.0$, $h=3.0$, and $T=1.0$. (c) A mixed phase region ($\rm AF_{1/2}+P$) for $\alpha=-0.1$, $d=-3.0$, $h=1.7$, and $T=0.1$. (d) A mixed phase region ($\rm AF_{1/2}+AF_{3/2}+AF_{5/2}$) for $\alpha=-0.1$, $d=-1.9$, $h=0.4$, and $T=0.2$.

3.2. Thermal behavior of the dynamic sublattice magnetizations

In order to find the dynamic phase boundaries among the phases, it is necessary to calculate the dynamic phase transition (DPT) temperatures. The DPT temperatures will be obtained by investigating the thermal behavior of the dynamic sublattice magnetizations. Moreover, from this investigation, the nature of phase transitions (continuous or discontinuous) will be characterized.

The dynamic sublattice magnetizations $(M_{\rm A},M_{\rm B})$ are defined as

$$M_{\rm A}=\frac{1}{2\pi}\int_0^{2\pi} m_{\rm A}(\xi)\,{\rm d}\xi, \tag{13a}$$

and

$$M_{\rm B}=\frac{1}{2\pi}\int_0^{2\pi} m_{\rm B}(\xi)\,{\rm d}\xi. \tag{13b}$$

Equations 13(a) and 13(b) are solved by combining the numerical methods of Adams–Moulton predictor–corrector method with the Romberg integration. The behaviors of the $M_{\rm A}$ and $M_{\rm B}$ as a function of the temperature for several values of the interaction parameters are given in Figs. 2(a)–2(e). In these figures, $T_{\rm c}$ and $T_{\rm t}$ are the critical or the second-order (also called Neel temperature) and the first-order phase transition temperatures, respectively. Figure 2(a) shows the thermal behavior of $M_{\rm A}$ and $M_{\rm B}$ for $\alpha=-0.5$,

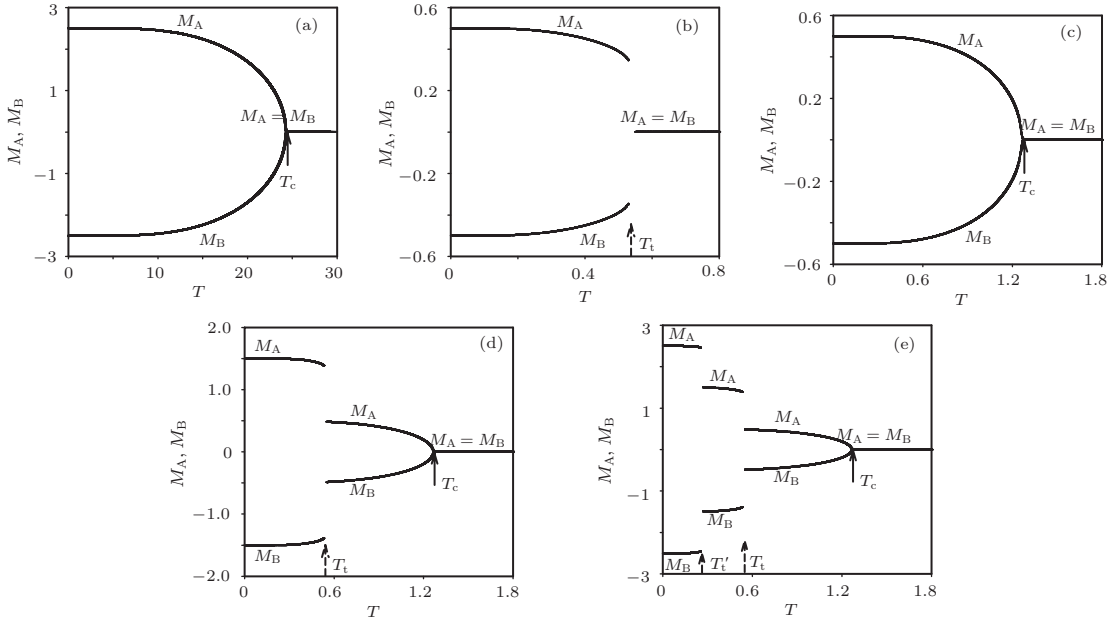


Fig. 2. Thermal behavior of the dynamic sublattice magnetizations (M_A,M_B). (a) A second-order phase transition from the $AF_{5/2}$ phase to the P phase for $\alpha = -0.5$, $d = 5.0$ and $h = 4.0$, and T_c is found to be 24.35. (b) A first-order phase transition from the $AF_{1/2}$ phase to the P phase for $\alpha = -0.5$, $d = -4.0$, and $h = 2.3$, and T_t is found to be 0.55. (c) A second-order phase transition from the $AF_{1/2}$ phase to the P phase for $\alpha = -0.1$, $d = -2.5$, and $h = 0.2$ and the initial values of M_A and M_B are taken as 0.5 and -0.5; T_c is found to be 1.27. (d) Two successive phase transitions, the first one is a first-order phase transition from the $AF_{3/2}$ phase to the $AF_{1/2}$ phase and the second one is a second-order phase transition from the $AF_{1/2}$ phase to the P phase for $\alpha = -0.1$, $d = -2.5$, and $h = 0.2$ and the initial values of M_A and M_B are taken as 1.5 and -1.5; T_t and T_c are found to be 0.55 and 1.27, respectively. (e) Three successive phase transitions. The first one is a first-order phase transition from the $AF_{5/2}$ phase to the $AF_{3/2}$ phase, the second one is also a first-order phase transition from the $AF_{3/2}$ phase to the $AF_{1/2}$ phase, and the third one is a second-order phase transition from the $AF_{1/2}$ phase to the P phase for $\alpha = -0.1$, $d = -2.5$, and $h = 0.2$ and the initial values of M_A and M_B are taken as 2.5 and -2.5; T_t', T_t and T_c are found to be 0.26, 0.55, and 1.27, respectively.

$d = 5.0$, and $h = 4.0$. In this figure, $M_A = 5/2$ and $M_B = -5/2$ at zero temperature and as the temperature increases, M_A decreases, and M_B increases continuously and they meet at T_c. Hence, a second-order phase transition occurs at $T_c = 24.35$ and the transition is from the $AF_{5/2}$ phase to the P phase. Figure 2(b) presents the existence of T_t when $\alpha = -0.5$, $d = -4.0$, and $h = 2.30$. In this figure, $M_A = 1/2$ and $M_B = -1/2$ at zero temperature and as the temperature increases, M_A decreases and M_B increases until they make jumps to zero at T_t. Then, M_A and M_B are always zero. Therefore, the system undergoes first-order phase transition at $T_t = 0.55$, because the discontinuity occurs for M_A and M_B and transition is from the $AF_{1/2}$ phase to the P phase. Neither solution does depend on initial values. Figures 2(c)–2(e) illustrate the thermal behavior of the M_A and M_B for $\alpha = -0.1$, $d = -2.50$, $h = 0.20$, and three different initial values; i.e., the initial values are taken as $M_A = 1/2$, $M_B = -1/2$ for Fig. 2(c), $M_A = 3/2$, $M_B = -3/2$ for Fig. 2(d) and $M_A = 5/2$, $M_B = -5/2$ for Fig. 2(e). Figure 2(c) is similar to Fig. 2(a), but in this case, the phase transition is from the $AF_{1/2}$ phase to the P phase at $T_c = 1.27$. In Fig. 2(d), the system undergoes two successive phase transitions: the first one is first order, because the discontinuity occurs for the M_A and M_B at $T_t = 0.55$. Transition is from the $AF_{3/2}$ phase to the $AF_{1/2}$ phase. The second one is second order from the $AF_{1/2}$ phase to the P phase at $T_c = 1.27$. Finally, in Fig. 2(e), the system undergoes three successive phase transitions: The first one is a first-order transition from the $AF_{5/2}$ phase to the $AF_{3/2}$ phase at $T_t' = 0.26$, the second one is also a first-order transition from the $AF_{3/2}$ phase to the $AF_{1/2}$ phase at $T_t = 0.55$, and the third one is a second-order phase transition from the $AF_{1/2}$ phase to the P phase at $T_c = 1.27$. From these figures, it is clearly seen that the system exhibits $AF_{1/2} + AF_{3/2} + AF_{5/2}$ and $AF_{1/2} + AF_{3/2}$ mixed phase regions until $T_t' = 0.26$ and $T_t = 0.55$, respectively. This fact is seen in the phase diagram of Fig. 3(d) explicitly, by comparing in Figs. 2(c)–2(e) with Fig. 3(d). In Figs. 2(c)–2(e), the obtained solutions depend on the initial values of M_A and M_B.

3.3. Dynamic phase diagrams

Since the DPT temperatures among the existing phases have been obtained in the previous section, now, the dynamic phase diagrams of the kinetic metamagnetic spin-5/2 Blume–Capel (BC) model can be presented. The calculated dynamic phase diagrams are presented in the (T,h), (d,T), $(-\alpha,T)$, (d,h), and $(-\alpha,h)$ planes in Figs. 3–7, respectively for the various values of interaction parameters. In these dynamic phase diagrams, the second-order phase transition temperatures indicated with solid lines and the first-order phase transition temperatures are shown with dashed lines. The dynamic tricritical point is the point at which solid and dashed lines are combined and denoted with filled circle.

Figure 3 shows the dynamic phase diagrams in the (T,h) plane for the various values of d and α and eight main topological dynamic phase diagrams are found. The set of

range of d and α parameters for the dynamic phase diagrams in this plane is given in Table 1. If one investigate these dynamic phase diagrams, one can observe following interesting results. (i) All phase diagrams exhibit one dynamic tricritical point. (ii) The dynamic triple point (TP) is observed only in Fig. 3(e) that three stable solutions or phases coexist in the system. (iii) The dynamic phase boundary between the paramagnetic and antiferromagnetic phases is usually second-order phase transition lines. On the other hand, the boundaries between the paramagnetic and mixed phases and between the antiferromagnetic and mixed phases are first-order phase transition line.

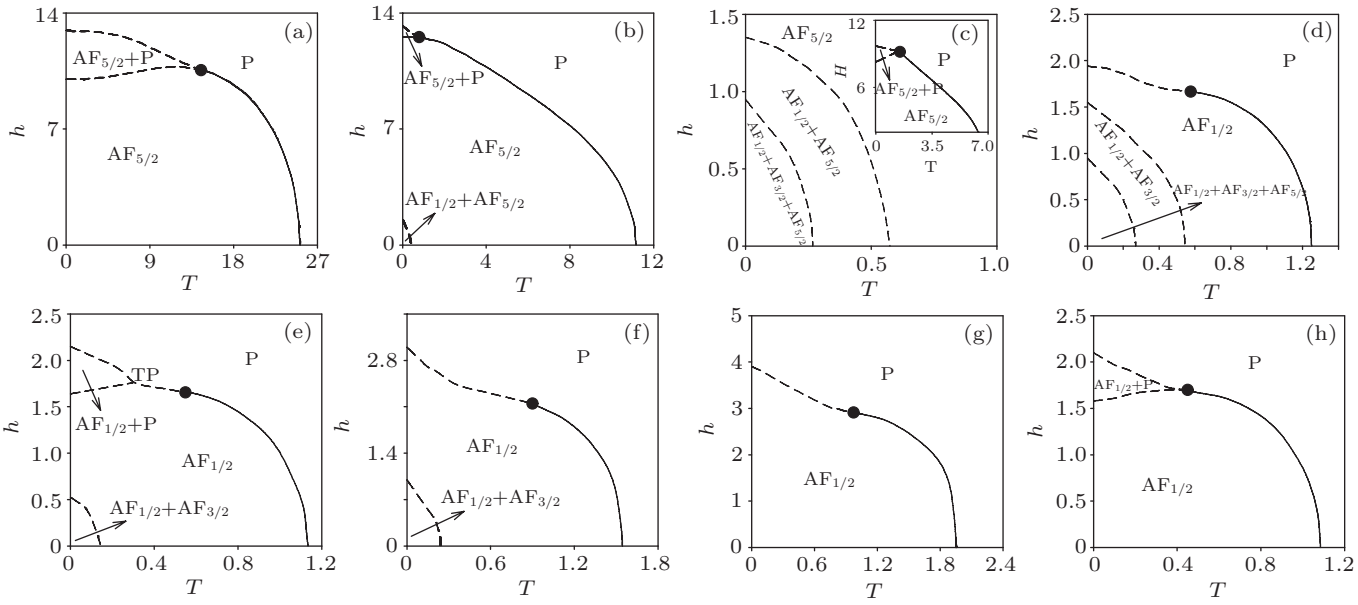


Fig. 3. Dynamic phase diagrams of the kinetic metamagnetic spin-5/2 Blume–Capel (BC) model in the (T,h) plane. Dashed and solid lines are the dynamic first- and second-order phase transition lines, respectively. The dynamic tricritical point is indicated with filled circle (•). TP is the dynamic triple point. (a) $\alpha=-0.5$ and $d=5.0$, (b) $\alpha=-0.5$ and $d=-2.2$, (c) $\alpha=-0.1$ and $d=-1.9$, (d) $\alpha=-0.1$ and $d=-2.5$, (e) $\alpha=-0.1$ and $d=-3.0$, (f) $\alpha=-0.5$ and $d=-4.0$, (g) $\alpha=-0.95$ and $d=-6.0$, (h) $\alpha=-0.1$ and $d=-11.0$.

Table 1. The set of range of d and α parameters for the dynamic phase diagrams in the (T,h) plane.

Figure	Set of range of d and α parameters
3(a)	for $\alpha=-0.5$, $d\geq-1.5676$; for $d=5.0$, every α values
3(b)	for $\alpha=-0.5$, $-1.5676>d\geq-2.3125$; for $d=-2.2$, $-0.4250\geq\alpha\geq-1.1250$
3(c)	for $\alpha=-0.1$, $-1.7074>d\geq-2.1972$; for $d=-1.9$, $0.0\geq\alpha\geq-2.2277$
3(d)	for $\alpha=-0.1$, $-2.1972>d\geq-2.6926$; for $d=-2.5$, $-0.0226\geq\alpha\geq0.2501$
3(e)	for $\alpha=-0.1$, $-2.6926>d\geq-3.1624$; for $d=-3.0$, $-0.0455\geq\alpha\geq-0.4250$
3(f)	for $\alpha=-0.5$, $-3.1320>d\geq-4.2455$; for $d=-4.0$, $-0.4172\geq\alpha\geq-0.9055$
3(g)	for $\alpha=-0.95$, $d\leq-3.9025$; for $d=-6.0$, every α values
3(h)	for $\alpha=-0.1$, $d<-3.1624$; for $d=-11.0$, $0.0\geq\alpha\geq-0.8950$

Figure 4 illustrates the dynamic phase diagrams in the (d,T) plane for various values of α and h parameters and five main different topological types of dynamic phase diagrams are seen. The set of range of α and h parameters for the dynamic phase diagrams in this plane is given in Table 2. The following interesting phenomena have been observed from these phase diagrams. (i) The dynamic tricritical point is only seen in the phase diagram of Fig. 4(b). (ii) The system exhibits one or two dynamic TPs (see Figs. 4(b)–4(e)). (iii) Figure 4(e) contains a dynamic quadruple point (QP) where four stable solutions coexist. (iv) Figures 4(c)–4(e) display interesting dynamic critical point. This point might be called a double critical end point (B) due to the reason that two different critical phases coexist. This point occurs for negative values of d in the system. (v) All dynamic phase boundaries among the mixed phases are first-order phase transition line.

Figure 5 represents the dynamic phase diagrams in the $(-\alpha,T)$ plane for various values of d and h parameters and six different phase topologies are obtained. The set of range of d and h parameters for the dynamic phase diagrams in this plane is given in Table 3. The basic properties of these phase diagrams are given as follows. (i) Figures 5(b) and 5(e) contain one dynamic tricritical point. (ii) The phase diagrams display one or two dynamic TPs (see Figs. 5(b), 5(d), and 5(e)). (iii) The dynamic B appears in Fig. 5(d). (iv) In Figs. 5(c) and 5(d), the filled triangle corresponds to the separating point which

separates the $AF_{1/2}$ phase from the $AF_{5/2}$ phase. This point has been observed previously in different systems.[50–58] (v) In Figs. 5(a) and 5(f), the dynamic phase boundary between the phases is only a second-order phase transition line. The mixed phases are separated from each other first-order phase transition line.

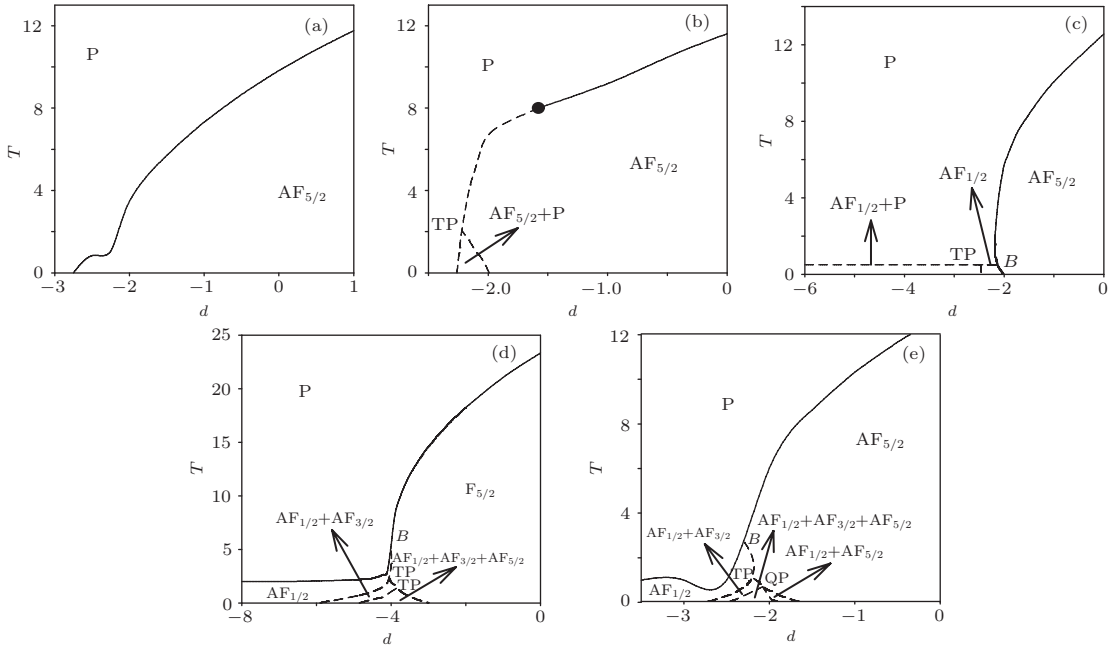


Fig. 4. Same as Fig. 3, but in the (d, T) plane. QP and B are the dynamic quadruple point and the dynamic double critical end point, respectively. (a) $\alpha = -0.1$ and $h = 6.0$, (b) $\alpha = -0.1$ and $h = 4.0$, (c) $\alpha = -0.1$ and $h = 2.0$, (d) $\alpha = -0.1$ and $h = 1.0$, (e) $\alpha = -1.0$ and $h = 0.1$.

Table 2. The set of range of α and h parameters for the dynamic phase diagrams in the (d, T) plane.

Figure	Set of range of α and h parameters
4(a)	for $h = 6.0$, $\alpha < -0.0041$; for $\alpha = -0.1$, $h > 4.2852$
4(b)	for $h = 4.0$, $-0.06398 \geq \alpha \geq -0.1455$; for $\alpha = -0.1$, $2.0945 < h \leq 4.2852$
4(c)	for $h = 2.0$, $-0.0523 \geq \alpha \geq -0.3460$; for $\alpha = -0.1$, $1.8750 < h \leq 2.0945$
4(d)	for $h = 1.0$, every α values; for $\alpha = -0.1$, $h \leq 1.8750$
4(e)	for $h = 0.1$, every α values; for $\alpha = -0.1$, $h \leq 3.3831$

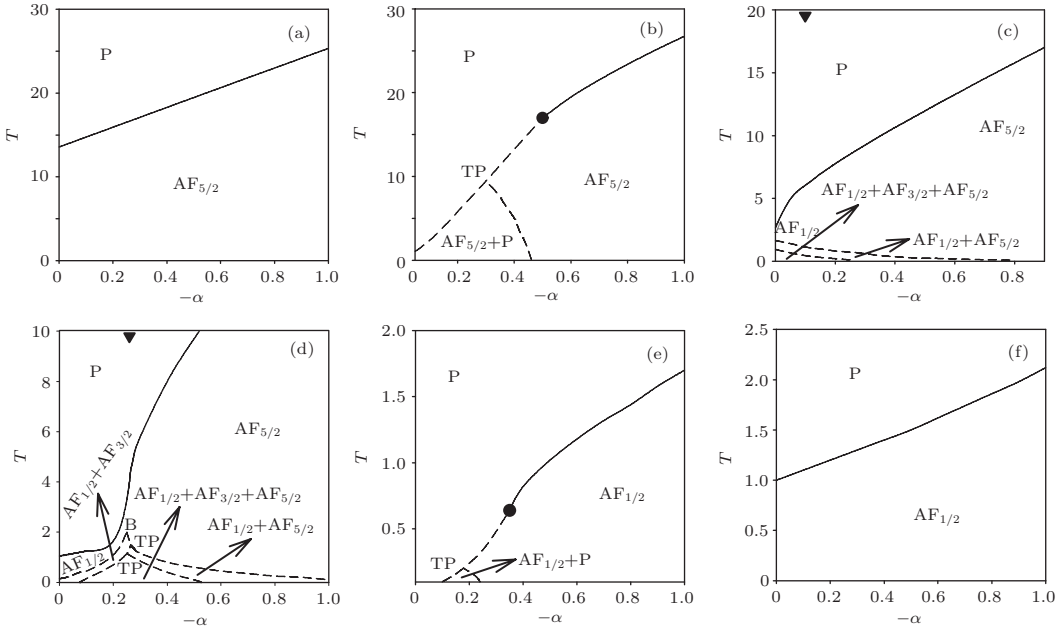


Fig. 5. Same as Fig. 3, but in the $(-\alpha, T)$ plane. The filled triangle (▼) separates the $AF_{1/2}$ phase from the $AF_{5/2}$ phase. (a) $d = 1.0$ and $h = 0.1$, (b) $d = 5.0$ and $h = 10.0$, (c) $d = -2.0$ and $h = 0.1$, (d) $d = -2.50$ and $h = 0.7$, (e) $d = -11.0$ and $h = 2.0$, (f) $d = -5.0$ and $h = 0.1$.

Table 3. The set of range of d and h parameters for the dynamic phase diagrams in the $(-\alpha, T)$ plane.

Figure	Set of range of d and h parameters
5(a)	for $h = 0.1$, $d \geq -1.3128$; for $d = 1.0$, $h \leq 8.3872$
5(b)	for $h = 10.0$, $d \geq -1.3825$; for $d = 5.0$, $h \geq 9.3440$
5(c)	for $h = 0.1$, $-1.3128 > d \geq -2.1682$; for $d = -2.0$, $h \leq 1.2371$
5(d)	for $h = 0.7$, $-2.0348 \geq d \geq -3.1304$; for $d = -2.5$, $h \leq 2.1104$
5(e)	for $h = 2.0$, $d \leq -2.5236$; for $d = -11.0$, $1.7973 \leq h \leq 2.8872$
5(f)	for $h = 0.1$, $d \leq -2.3895$; for $d = -5.0$, $h \leq 1.7972$

The calculated dynamic phase diagrams in the (d, h) plane are presented in Fig. 6 for various values of α and T parameters and five different phase diagrams are found. The set of range of the α and T parameters for the dynamic phase diagrams in this plane is given in Table 4. If one investigate these dynamic phase diagrams, one can observe the following interesting main results. (i) The phase diagrams exhibit one or two dynamic tricritical points. (ii) One, two, or three dynamic TPs occur in the system for negative values of d. (iii) One dynamic QP is observed in Figs. 6(d) and 6(e). (iv) Fig. 6(e) contains the dynamic B, but the others do not. (v) In Fig. 6(c), the filled triangle separates the $AF_{1/2}$ phase from the $AF_{5/2}$ phase at low values of h. (vi) In Fig. 6(a), the dynamic phase boundary is only second-order phase transition line, which separates the $AF_{5/2}$ phase from the P phase. In Fig. 6(e), all phase boundaries among the phases are first-order phase transition line.

Finally, figure 7 shows the dynamic phase diagrams in the $(-\alpha, h)$ plane for various values of d and T parameters and six different phase topologies are obtained. The set of range of d and T parameters for the dynamic phase diagrams in this plane is given in Table 5. The following main results have been observed from these phase diagrams. (i) Figure 7(a) displays the dynamic tricritical point at high values of h. (ii) In Fig. 7(e), the dynamic TP occurs in the system. (iii) In Fig. 7(f), the dynamic phase boundary is a second-order phase line, which separates the $AF_{1/2}$ phase from the P phase. In Figs. 7(b)–7(e), all dynamic phase boundaries among the phases are first-order phase transition line. In Fig. 7(a), the dynamic phase boundary between the $AF_{5/2}$ and P phases is a second-order phase line at low values of h and a first-order phase line at high values of h.

It should be mentioned that very similar phase diagrams to Figs. 3, 4(a), 5(a), 5(f), 6(a), 6(b), 7(a), 7(b), and 7(f) were obtained in kinetic spin systems with different spins.[28,49,56–58] On the other hand, the dynamic phase diagrams in Figs. 4(b)–4(e), 5(b)–5(e), 6(c)–6(e), and 7(c)–7(e) are new phase diagrams, which were obtained for only this system.

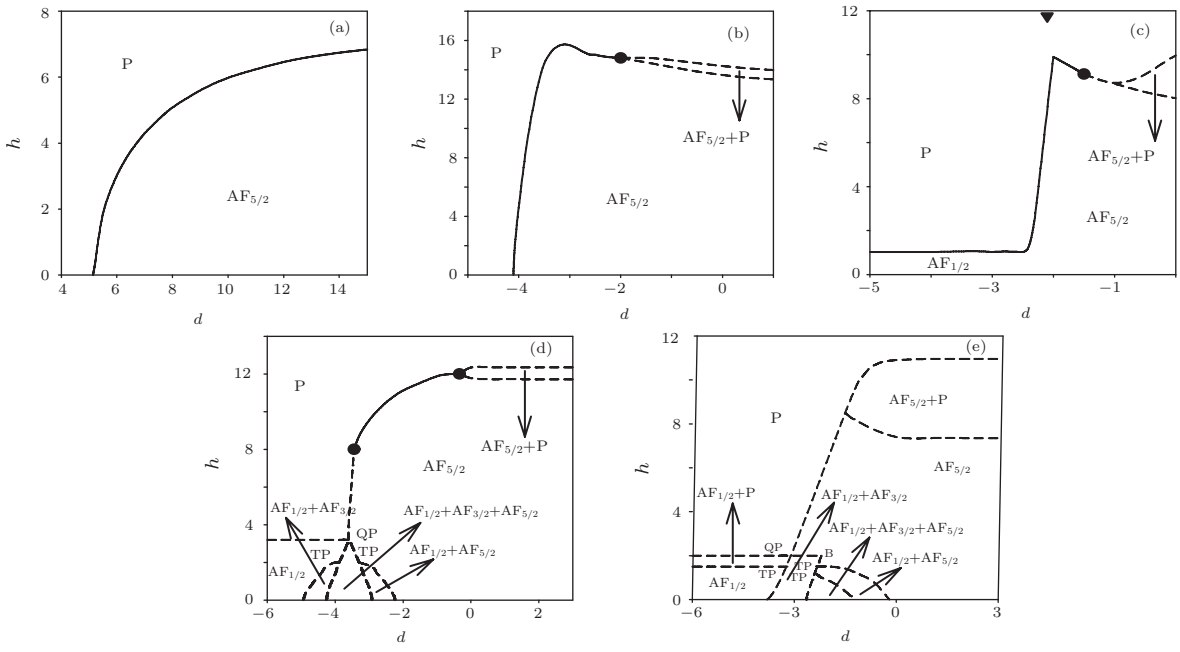


Fig. 6. Same as Fig. 3, but in the (d, h) plane. (a) $\alpha = -0.1$ and $T = 20.0$, (b) $\alpha = -1.0$ and $T = 4.0$, (c) $\alpha = -0.1$ and $T = 1.0$, (d) $\alpha = -0.8$ and $T = 0.2$, (e) $\alpha = -0.1$ and $T = 0.1$.

Table 4. The set of range of α and T parameters for the dynamic phase diagrams in the (d,h) plane.

Figure	Set of range of α and T parameters
6(a)	for $T = 20.0$, $\alpha \geq -0.5998$; for $\alpha = -0.1$, $T > 13.169$
6(b)	for $T = 4.0$, every α values; for $\alpha = -1.0$, $T \geq 3.253$
6(c)	for $T = 1.0$, $\alpha \geq -0.8082$; for $\alpha = -0.1$, $0.5036 < T \leq 13.169$
6(d)	for $T = 0.2$, $\alpha \leq -0.7475$; for $\alpha = -0.8$, $0.1675 \leq T \leq 0.9537$
6(e)	for $T = 0.1$, $\alpha \geq -0.8995$; for $\alpha = -0.1$, $T \leq 0.5036$

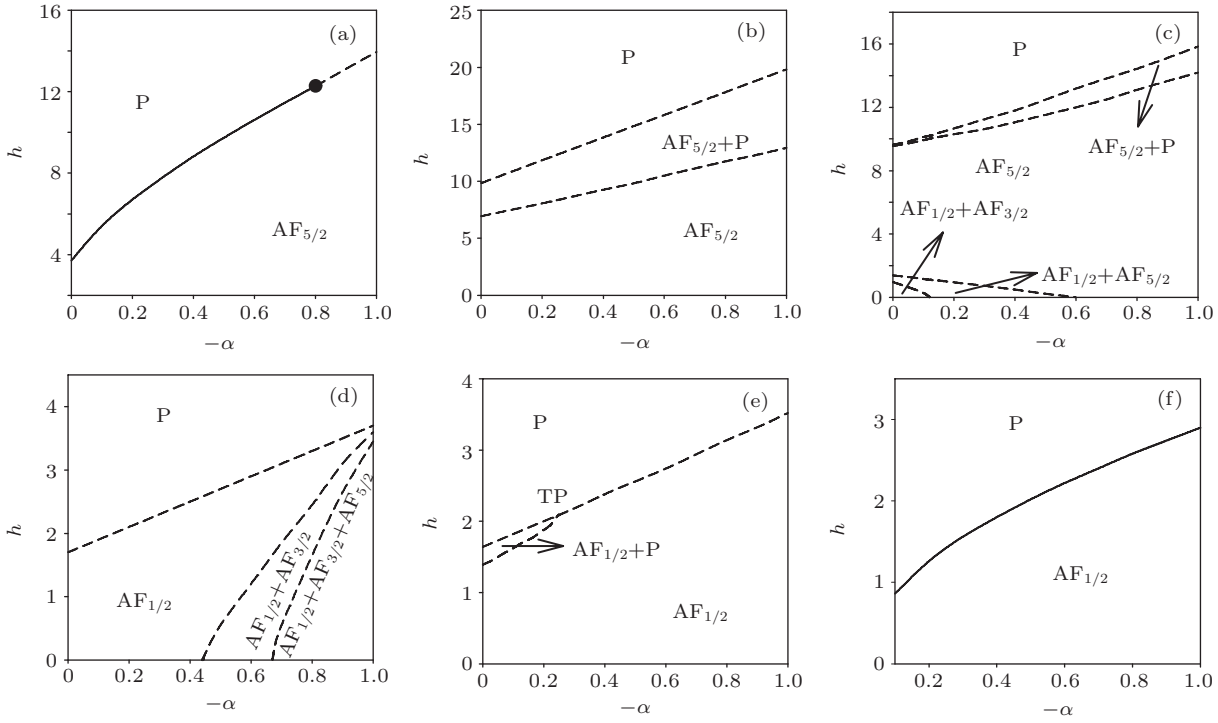


Fig. 7. Same as Fig. 3, but in the $(-\alpha,h)$ plane. a) $d = -1.0$ and $T = 8.0$, (b) $d = 2.0$ and $T = 0.250$, (c) $d = -1.80$ and $T = 0.1$, (d) $d = -4.0$ and $T = 0.15$, (e) $d = -10.0$ and $T = 0.25$, (f) $d = -11.0$ and $T = 1.0$.

Table 5. The set of range of d and T parameters for the dynamic phase diagrams in the $(-\alpha,h)$ plane.

Figure	Set of range of d and T parameters
7(a)	For $T = 8.0$, $-3.9115 \leq d \leq 2.1412$; for $d = -1.0$, $1.6750 \leq T \leq 9.1201$
7(b)	For $T = 0.25$, $d \geq -1.4629$; for $d = 2.0$, $T \leq 7.9375$
7(c)	For $T = 0.1$, $-1.9352 \leq d \leq 1.6116$; for $d = -1.8$, $0.0 \leq T \leq 0.3650$
7(d)	For $T = 0.15$, $-5.6260 \leq d \leq -2.6799$; for $d = -4.0$, $T \leq 2.1012$
7(e)	For $T = 0.25$, $d \leq -2.5368$; for $d = -10.0$, $T \leq 0.4391$
7(f)	For $T = 1.0$, $d \leq -2.1163$; for $d = -11.0$, $0.5038 \leq T \leq 1.9733$

4. Summary

In this work, the nonequilibrium or dynamic phase transitions of the kinetic metamagnetic spin-5/2 Blume–Capel model in the presence of a time-dependent oscillating external magnetic field have been investigated. The time evolution of the system was described by a stochastic dynamics of the Glauber type. By using the master equation, the dynamic mean-field equations of the system have been obtained. The time variations of the order parameters are investigated to find the phases in the system. As a result of this investigation, it has been found that the system exhibits two solutions or phases: paramagnetic (P) and antiferromagnetic ($AF_{5/2}$, $AF_{3/2}$, and $AF_{1/2}$). Moreover, the system contains five mixed phase regions ($AF_{5/2}+P$, $AF_{1/2}+P$, $AF_{1/2}+AF_{3/2}$, $AF_{1/2}+AF_{5/2}$, and $AF_{1/2}+AF_{3/2}+AF_{5/2}$) composed of binary and ternary combination of these phases. The mixed phase regions usually occur at low values of the temperature. Then, the thermal behavior of the order parameters in a period, also called the dynamic order parameters, are studied in order to characterize the nature of phase transitions and to obtain the dynamic phase

transition (DPT) temperatures. After all these investigations, the dynamic phase diagrams have been presented in the (T,h), (d,T), $(-\alpha,T)$, (d,h) and $(-\alpha,h)$ planes for different values of the interaction parameters. The system also displayed many dynamic critical points, such as tricritical, triple point (TP), quadruple point (QP), double critical end point (B), and separating point.

Finally, we should emphasize that this mean-field dynamic study, in spite of its limitations, e.g., the correlation of spin fluctuations have not been considered, suggests that kinetic metamagnetic spin-5/2 Ising model has an interesting dynamic behavior and gives rich dynamic phase diagrams. It is quite different from the standard Ising model, and it would be worthwhile to further explore it by using nonperturbative methods such as kinetic Monte–Carlo simulations or renormalization-group calculations. Moreover, our results will be instructive in the time-consuming process of searching the critical behavior of this system while using the dynamic MC simulations, as well as they may give some light for experimental works.

References

[1] Kincaid J M and Cohen E G D 1975 *Phys. Rep. C* **22** 57
[2] Birgeneau R J, Yelon W B, Cohen E and Makovsky J 1972 *Phys. Rev. B* **5** 2607
[3] Wilkinson M K, Cable J W, Wollan E O and Koehler W C 1959 *Phys. Rev.* **113** 497
[4] Stryjewski E and Giordano N 1977 *Adv. Phys. B* **26** 487
[5] Selke W 1995 *Z. Phys.* B **101** 145
[6] Zuković M and Bobák A 1997 *J. Magn. Magn. Mater.* **179** 49
[7] Zuković M, Bobák A and Idogaki T 1998 *J. Magn. Magn. Mater.* **188** 52
[8] Zuković M, Bobák A and Idogaki T and Branco N S 1999 *J. Magn. Magn. Mater.* **192** 363
[9] Zuković M and Idogaki T 2000 *Phys. Rev. B* **61** 50
[10] Galam S and Salinas S R 2002 *Phys. Rev. B* **66** 060402
[11] Liu J, Wei G and Miao H 2007 *J. Magn. Magn. Mater.* **315** 101
[12] Geng J and Wei G 2009 *J. Magn. Magn. Mater.* **321** 1964
[13] Geng J, Wei G and Miao H 2008 *J. Magn. Magn. Mater.* **320** 2171
[14] Oliveira de D C, Silva da A A P, Albuquerque de D F and Arruda de A A 2007 *Physica A* **336** 205
[15] Filho E B and Sousa de J 2004 *Phys. Lett. A* **323** 9
[16] Guimaras E S and Albuquerque E L 2003 *J. Phys. Condens. Matter* **307** 172
[17] Sieger M, Kasten A and Paul W 1985 *Solid State Commun.* **53** 909
[18] Yang Z R 1992 *Phys. Rev. B* **46** 11578
[19] Glauber R J 1963 *J. Math. Phys.* **4** 294
[20] Zuković M and Idogaki T 2000 *J. Magn. Magn. Mater.* **208** 120
[21] Sahni P S, Gunton J D, Sheldon L K and Timpe R H 1998 *Phys. Rev. B* **57** 389
[22] Oğuz E 1988 *J. Phys. A* **21** 2799
[23] Santos M and Figueiredo W 1997 *Phys. Rev. B* **55** 11353
[24] Das D and Barma M 1999 *Physica A* **270** 245
[25] Gülpınar G, Demırhan D and Büyükkılıç 2007 *Physica A* **383** 372
[26] Gülpınar G, Demırhan D and Büyükkılıç F 2009 *J. Stat. Phys.* **373** 511
[27] Keskin M, Canko O and Kantar E 2009 *Phys. Lett. A* **373** 2201
[28] Keskin M, Canko O and Kırak M 2007 *Phys. Stat. Sol. B* **244** 3775
[29] Kırak M, Canko O and Keskin M 2009 *Z. Naturforsch.* **64a** 185
[30] Gülpınar G 2008 *Phys. Lett. A* **372** 98
[31] Deviren B and Keskin M 2010 *Phys. Lett. A* **374** 3119
[32] Acharyya M 2011 *J. Magn. Magn. Mater.* **323** 2872
[33] Gülpınar G and Vatansever E 2012 *J. Magn. Magn. Mater.* **324** 983
[34] Plascak J A, Moreira J G and Barretosá F C 1993 *Phys. Lett. A* **173** 360
[35] Kaneyoshi T and Jaščur 1993 *Phys. Stat. Sol. B* **175** 225
[36] Benyoussef A 1993 *Phys. Stat. Sol. B* **178** 233
[37] Kerouad M, Saber M and Tucker J W 1994 *Physica A* **210** 424
[38] Song W J and Yang C Z 1994 *Solid State Commun.* **92** 361
[39] Lee Y S, Greven M, Wells B O, Birgeneau B J and Shirane G 1998 *Eur. Phys. J. B* **5** 15
[40] He Z, Ueda Y and Itoh M 2007 *Solid State Commun.* **141** 22
[41] Cowley R A, Aharony A, Birgeneau R J, Pelcovits R A, Shirane G and Thurston T R 1993 *Z. fuer Phys. B* **93** 5
[42] Cowley R A, Shirane G, Birgeneau R J and Guggenheim H J 1977 *Phys. Rev. B* **15** 429
[43] Costa B V and Pires A S T 2003 *J. Magn. Magn. Mater.* **262** 316
[44] Christianson R J, Leheny R L, Birgeneau R J and Erwin R W M 2001 *Phys. Rev. B* **63** 140401
[45] Wildes A R, Rønnow H M, Roeesli B, Haris M J and Godfrey K W 2006 *Phys. Rev. B* **74** 094422
[46] Deviren B, Keskin M and Canko O 2009 *J. Math. Phys.* **82** 693
[47] Ertas M and Keskin M 2010 *Phase Trans.* **83** 349
[48] Ertaş M, Keskin M and Deviren B 2012 *J. Magn. Magn. Mater.* **324** 1503
[49] Temizer Ü and Özkılıç A 2013 *Chin. Phys. B* **22** 037501
[50] Keskin M and Kantar E 2010 *J. Magn. Magn. Mater.* **322** 2789
[51] Deviren B and Keskin M 2009 *J. Stat. Phys.* **140** 934
[52] Canko O, Deviren B and Keskin M 2008 *JETP Lett.* **87** 633
[53] Keskin M and Ertas M 2009 *Phys. Rev. E* **80** 061140
[54] Deviren B, Canko O and Keskin M 2009 *J. Magn. Magn. Mater.* **321** 1231
[55] Strečka J 2006 *J. Magn. Magn. Mater.* **360** 379
[56] Özkılıç A and Temizer Ü 2013 *J. Magn. Magn. Mater.* **330** 55
[57] Korkmaz T and Temizer Ü 2012 *J. Magn. Magn. Mater.* **324** 3876
[58] Temizer Ü and Korkmaz T 2012 *Eur. Phys. J. B* **85** 330